First-principles studies on magnetic properties of freestanding CrB_2 films

Hui Zhao[1,a], *Yan Zhao[1,b], Yining Zhang[1,c], Qian Han[2,d]

[1]Department of Physics, Anshan Normal University, Anshan 114007, China

[2]Department of chemistry, Anshan Normal University, Anshan 114007, China

[a] hzhao@aliyun.com, [b]971967125@qq.com, [c]yining303@126.com, [d]chem_qianhan@126.com

Keywords: CrB_2 film; first-principles; electronic structure; magnetism; Mulliken population

Abstract. Atomic and electronic structures of CrB_2 (0001) freestanding ultrathin films are investigated using first-principles total energy plane-wave pseudopotential method based on density functional theory. The slab models are simulated for both Cr termination and B termination with different slab thickness. For both terminations, the interlayer spacings are contracted in most of the interlayer region. The outermost interlayer contraction of Cr-terminated films is quite large, while the B-terminated films' is relatively small. Moreover, we found that the magnetism of CrB_2 is stable for the models with different slab thickness. It suggests that changing of slab thickness does not significantly influence the magnetic properties of CrB_2 thin films. The stable magnetism of ultrathin CrB2 film with slab thickness of three atomic layers also indicates that it may be meaningful and useful for spintronic applications in forms of films and layers.

Introduction

Low dimensional systems including surfaces, interfaces and thin-films, have attracted a great amount of attention in the past decade because, as expected, the lowered symmetry and coordination number offer a variety of opportunities for inducing new and exotic phenomena and so hold out the promise of new device applications. Graphene, a carbon honeycomb with only one-atom thickness isolated from graphite in 2004, is the first example of true two-dimensional (2D) single-layer atomic crystal [1]. Despite its short history, graphene shows tremendous attraction to researchers from different fields because of its exceptional properties and has risen as the most exciting star in materials science during the past several years [2]. As a matter of fact, the intensive studies on graphene have sparked new discoveries towards graphene-analogous materials, comprising single layer or few layers with compositions other than carbon [3-5]. Initially, following the same micromechanical exfoliation methodology originally used in graphite, Novoselov *et al*. [6] successfully isolated individual single layers from a large variety of layered materials including h-BN, dichalcogenides (such as MoS_2 and $NbSe_2$) and complex oxides (such as $Ba_2Sr_2CaCu_2O_x$). Since then, many 2D materials including BC_3 [7], MXene (transition metal carbides and nitrides, such as Ti_3C_2 [8] and Ti_2C [9]), and coordination polymers (such as $[Cu_2Br(IN)_2]_n$ [10] and polymeric Fe-phthalocyanine [11]), have been prepared and characterized, and new fabrication methods, including liquid-phase exfoliation [12], electrochemical exfoliation [13], chemical vapor deposition, and polycondensation reaction, have been accordingly established.

With the help of recent advanced progress in thin film deposition such as molecular beam epitaxy and pulsed laser deposition, many novel compounds have been grown and synthesized in the forms of films and layers. Silicene has been successfully fabricated on several substrates such as silver, zirconium diboride, and iridium [14-17]. Li *et al*. show that 2D honeycomb lattice structures can also be created using transition metal atoms such as hafnium [18-19]. Moreover, large-area graphene also provide a promising lab bench for synthesizing, manipulating, and characterizing low-dimensional materials, opening the door to high-resolution analyses of novel structures, such as 2D glasses, that cannot be exfoliated and may not occur naturally [20]. Zhao *et al*. show a freestanding crystalline single-atom-thick layer of iron and the work could pave the way for new 2D structures to be formed in graphene membranes [21].

The synthesis of novel 2D materials has attracted considerable interest due to their various unique properties. Boron is possibly the second element that can possess multiple low-dimensional allotropes. Nevertheless, the boron layer is very difficult to be prepared as a freestanding sheet, differently from graphene or BN sheet, on the ground that it lacks one electron per atom to form the stable sp^2 hybridization network by itself [22-23]. Although there are some studies that focus on the prediction of 2D boron, the theoretically predicted stable boron sheets do not adopt ideal honeycomb structure like graphene [24-25]. Many researches reveal that it is evident for charge transfer from the metal to the boron atoms helps to stabilize the sp^2 boron network [26-28]. The metal-boron interaction in the metal diborides plays an important role. Consequently, studying boron honeycomb in metal diborides surface containing a graphitic boron layer may be a feasible way [29-30]. The discovery of superconductivity at 39K in MgB_2 has attracted interest in investigating the properties of the metal diborides with hexagonal AlB_2-type structure [31]. AlB_2-type metal diborides are layered compounds with a hexagonal structure in which a graphene-like boron layer alternates with a close-packed metal layer. These materials have a unique combination of properties such as high melting point, hardness, chemical stability, high thermal conductivity, low electrical resistivity, and low work function [32-35], which attracts a number of researchers from different fields to elucidate their structures experimentally and theoretically and draw out their commercial potentials studiously [36-38].

Scientific and technical advances have created unprecedented new opportunities for designing artificial materials. Among them are epitaxially grown ultrathin films stabilized on various substrates. In our previous work, we introduced the superlattice engineering for achieving the possible binary *sp* half-metallic ferromagnets [39-40]. In present work, we introduce the ultrathin film engineering for realizing the hypothetical 2D boron sheets. In this paper, we will concentrate on CrB_2 (0001) freestanding ultrathin film out of many other materials due to its magnetic properties and potential applications for spintronics. CrB_2 has a complicated helicoidal magnetic structure by neutron diffraction measurements. But for simplicity, it is always assumed the ferromagnetic ordering in density functional calculations [26]. The geometric, electronic and magnetic properties as a function of slab thickness will be shown in this paper to help make a contribution to the fundamental understanding of the thickness dependent properties of the CrB_2 (0001) thin solid films.

Computational details

All calculations are performed using CASTEP code [41] based on the density functional theory [42-43], where the generalized gradient approximation plus on-site Coulomb repulsion Hubbard *U* (GGA+*U*) with the Perdew-Burke-Ernzerhof (PBE) scheme is adopted [44]. For the GGA+*U* calculations, *U*=6eV were applied to Cr 3*d* states and *U*= 4eV were applied to B 2*p* states [45-48]. The minimum total energy of the structure is achieved by relaxing automatically the internal coordinates using the Broyden-Fletcher-Goldfarb-Shanno (BFGS) algorithm [49]. The atomic configurations of Cr and B used to generate the ultrasoft pseudopotential are $3s^2 3p^6 3d^5 4s^1$ and $2s^2 2p^1$, respectively [50]. The wave functions are expanded with the plane-wave pseudopotentials, while the cutoff energy is set to be 310eV, which is sufficient in leading to a good convergence: the total energy difference within 10^{-5}eV/atom, the maximum Hellmann-Feynaman forces acting on the atoms within 0.03eV/Å , the maximum stress within 0.05GPa, and the maximum atom displacement within 10^{-3}Å. The special points sampling integration over the Brillouin zone is employed by the Monkhorst-Pack method [51] with *k*-point set 10×10×1 for the slab calculations. CrB_2 has a complicated helicoidal magnetic structure, as resolved by neutron diffraction measurements. But for simplicity, we have assumed the ferromagnetic ordering in bulk and slab models. Our calculations yielded the lattice constants of *a*=2.97348 Å and *c*=3.05276 Å for bulk CrB_2, which agrees well with other theoretical and experimental results [26]. All the following models and calculations are based on this bulk geometry. We have considered the symmetric (non-stoichiometric) slab models, which are used to eliminate the spurious dipole effects, since the polar CrB_2 (0001) is terminated with only one kind of atom Cr or B. The orientation of the films is chosen such that their surfaces

correspond to the most stable, simple surface of the respective bulk material. For CrB_2 (0001) freestanding films, 1×1 slab models with slab thickness of 3, 5, 7, 9 with two possible terminations and a 15Å vacuum layer have been considered. The perspective views of the atomic structures of the slab models are shown in Figure 1.

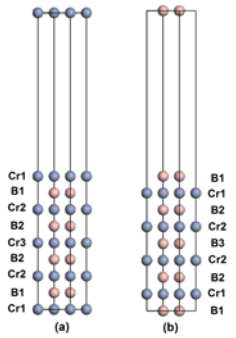

Figure 1. Schematic diagrams of (a) Cr-terminated and (b) B-terminated CrB_2 (0001) ultrathin films with nine layers. The grey spheres represent Cr atoms; the pink spheres represent B atoms.

Results and discussion

The results of the relaxation are shown in Table 1. The ratio of the change of the interlayer spacing Δ_{ij} is defined as [52-54]

$$\Delta_{ij} = \frac{\Delta d_{ij}}{d_0} = \frac{d_{ij} - d_0}{d_0},$$

where d_{ij} is the interlayer distance between the *i*th and *j*th layers and d_0 is the corresponding distance in bulk. Δd_{ij} is the change of the interlayer distance after full relaxation.

Table 1. CrB_2 (0001) slab relaxations as a function of termination and slab thickness (change of the interlayer spacing Δ_{ij} as a percentage of the spacing in the bulk).

Termination	Interlayer	Slab thickness, n			
		3	5	7	9
Cr	$\triangle_{12}$	-4.86	-9.96	-8.35	-8.47
	$\triangle_{23}$		-3.52	-0.86	-1.24
	$\triangle_{34}$			-0.69	-0.86
	$\triangle_{45}$				0
B	$\triangle_{12}$	-0.82	-0.04	-0.17	-0.46
	$\triangle_{23}$		-0.19	-1.68	-1.83
	$\triangle_{34}$			1.29	-0.05
	$\triangle_{45}$				1.34

From Table 1, one can see that, for both terminations, the interlayer spacings are contracted in most of the interlayer region. The outermost interlayer contraction of the Cr-terminated films is rather large even more than 9%, while the B-terminated films' is relatively small. The third interlayer distance of B-terminated slab with 7 atomic layers is enlarged by 1.29% of those in the bulk and the forth of 9 layer slab is enlarged by 1.34%. These results may suggest that the B-terminated films are more stable than the Cr-terminated films because of the smaller relaxations, which is similar to the relaxation behavior of group-V transition metal diboride surfaces and corresponding CrB_2 (0001) surfaces [55]. In bulk CrB_2, there are two types of bond, the σand π bonds, which are formed by hybridization of Cr *d* states, B *s* and *p* states [56]. The bonding in ultrathin films is in a more complicated situation because atoms at the surface of slab lose half of their neighboring atoms, charge will redistribute and the bonding will be perturbed. To help further understand the systems, the Mulliken population is calculated according to the formalism described by Segall *et al*. [57] to provide some valuable information about charge transfer and magnetic properties. Table 2 shows the effective atomic charges for both termination films with different slab thickness compared with unrelaxed ones.

Table 2. Mulliken charges (in units of |*e*|) for the relaxed and unrelaxed Cr-terminated and B-terminated CrB_2 (0001) thin films.

Termination	Layer	Charge							
		3		5		7		9	
		Relaxed	Unrelaxed	Relaxed	Unrelaxed	Relaxed	Unrelaxed	Relaxed	Unrelaxed
Cr	Cr1	0.62	0.59	0.64	0.57	0.63	0.57	0.63	0.57
	B1	-0.62	-0.59	-0.62	-0.59	-0.62	-0.60	-0.62	-0.60
	C2			1.19	1.22	1.15	1.17	1.15	1.17
	B2					-0.54	-0.55	-0.54	-0.55
	Cr3							1.10	1.12
B	B1	-0.39	-0.38	-0.38	-0.37	-0.38	-0.38	-0.38	-0.38
	Cr1	1.54	1.54	1.33	1.32	1.33	1.31	1.34	1.31
	B2			-0.57	-0.57	-0.57	-0.56	-0.57	-0.56
	Cr2					1.12	1.11	1.12	1.11
	B3							-0.55	-0.55

It is clear that charge transfers from Cr atoms to B atoms happened among all the layers. The calculated results show that the charge transfers between the top two layers for both terminations are trivially increased after full relaxation, while the effective charges of third to fifth layer atoms of Cr-terminated films are trivially decreased. Increase of charge transfers may strengthen the chemical bonds between B atoms. The B-B bond lengths in the second or first layer for Cr-terminated and B-terminated models are displayed in Table 3 to check the strengthen effect from charge redistribution and transfer. It is worth to note that, for Cr-terminated slabs, B-B lengths in the second layer are longer than that in the bulk (1.717Å); on the other hand, B-B lengths of B-terminated slabs in the first layer are shorter. The charge transfers from Cr atoms to B atoms only shorten the B-B bond lengths and strengthen the B-B networks for B-terminated films. This fact may also be the evidence that the B-terminated systems are more stable than the Cr-terminated systems as we suggested above. So far, we may draw a conclusion that, for Cr-terminated films, the charge transfers from Cr atoms to B atoms between the top two layers stabilize the boron networks by filling the B p_z states which strengthen the hybridization of B p_z and Cr 3*d* states. The strengthened B p_z-Cr 3*d* bonds pull the first two layers closer. But there is not enough electrons to fill the boron $2p_{x,y}$ states, which are responsible for the formation of B-B σbonds, and the B-B bond lengths of Cr-terminated films in the second layer are enlarged compared with those in the bulk. On the contrary, B-terminated films have enough electrons to fill the boron $2p_{x,y}$ states, the B-B σ bonds are enhanced and B-B bond lengths are reduced. Less contribution is made to the filling of the π bonds so the contractions of the outermost interlayer spacing of the B-terminated films are smaller. The difference between the two terminations may be contributed by the less effective charges provided by Cr atoms in the third layer of Cr-terminated films.

Table 3. B-B bond lengths (in units of |Å|) in the second or first layer for both termination films.

Termination	Layer	B-B bond length			
		3	5	7	9
Cr	2	1.738	1.751	1.738	1.736
B	1	1.673	1.692	1.696	1.696

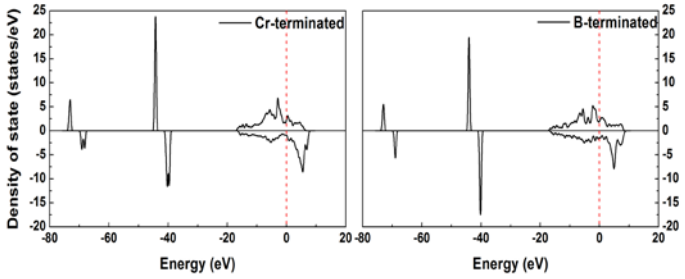

Figure 2. Total DOS for Cr-terminated and B-terminated CrB_2 (0001) ultrathin films with nine atomic layers.

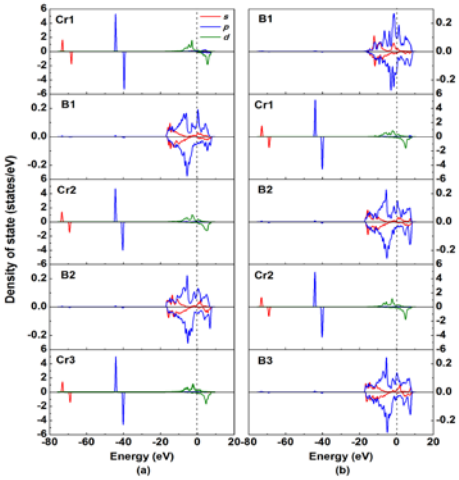

Figure 3. Layer resolved projected DOS for (a) Cr-terminated and (b) B-terminated CrB_2 (0001) ultrathin films with nine atomic layers.

Further elucidation from other aspects: the density of states and the electron charge density would be necessary. We select films with slab thickness of 9 as an example. The total and projected densities of states (DOS) of both terminations are shown in Figure 2 and 3. Despite their different terminations, the electronic structures for both systems are quite similar overall. These curves demonstrate that the metal- and boron-terminated films are all metallic. The largest contribution to the total DOS around Fermi level is *d* orbital electrons, *s* and *p* orbital electrons' contributions are relatively small. From Figure 2, there are two noticeable differences between the two systems: 1), the "pseudo-gap" existing in B-terminated system disappears in Cr-terminated system; 2), the peaks in the minority *s* and *p* spin states of Cr-terminated system around -40 and -70eV split into two. These effects are mainly contributed by the hybridization of Cr orbitals and B orbitals. For Cr-terminated slabs, more valence electrons transferring from Cr to B (see Table 2) will strengthen the hybridization and finally lower the energy of the bonding states, which cause the enhanced DOS at Fermi level. The hybridization of Cr minority *s* and *p* states in the nearest neighboring slabs is responsible for the splitting. We can also notice from the projected DOS that the magnetic moments of both systems are mainly contributed by the splitting of Cr electronic states. To quantify the magnetic properties of CrB_2 (0001) films, the atomic spin moments calculated from the Mulliken population analysis are given in Table 4. The magnetic moments of Cr in the first or second layer of Cr-terminated and B-terminated films become smaller after full relaxation, where *d* electrons are delocalized so that the exchange interaction between the majority and the minority spin states decreases.

In order to better understand the electronic structure of the ultrathin films, we plotted the spin density and difference charge density contour maps for both terminations to visualize the electronic and bonding properties of the systems. From spin density map (see Figure 4), it is evidence that, for both terminated models, the magnetism of the materials mainly comes from Cr atoms, which agree well with the Mulliken results. Figure 5 gives the charge density difference for Cr-terminated and B-terminated films between each slab and its corresponding isolated atoms. The more negative or blue the mark is in this figure, the more electrons the atoms lose. It is not surprising to observe that the electron density around Cr atoms is decreased while there is enhancement at each B atom. Obviously, there are charge transfers from Cr to B and Cr-B bonds have the character of ionic bonding. Also, significant charge accumulation between the boron atoms in the same layer indicates a strong covalent B-B bonding. The region of charge loss is mainly limited in Cr atoms and charge accumulation is mainly between the B atoms. The descriptions from the color maps are all consist with the Mulliken analysis above.

Table 4. Atomic magnetic moments (in units of $|\mu_B|$) for both termination films.

Termination	Layer	Magnetic Moment							
		3		5		7		9	
		Relaxed	Unrelaxed	Relaxed	Unrelaxed	Relaxed	Unrelaxed	Relaxed	Unrelaxed
Cr	Cr1	2.66	2.72	4.84	4.94	4.9	4.98	4.88	4.98
	B1	-0.4	-0.4	-0.4	-0.38	-0.4	-0.38	-0.42	-0.4
	C2			3.7	3.64	3.78	3.72	3.72	3.68
	B2					-0.36	-0.36	-0.36	-0.38
	Cr3							3.78	3.72
B	B1	-0.16	-0.18	-0.18	-0.14	-0.16	-0.18	-0.18	-0.2
	Cr1	3.64	3.86	3.7	3.8	3.64	3.74	3.62	3.74
	B2			-0.36	-0.38	-0.36	-0.38	-0.38	-0.38
	Cr2					3.76	3.74	3.7	3.72
	B3							-0.36	-0.38

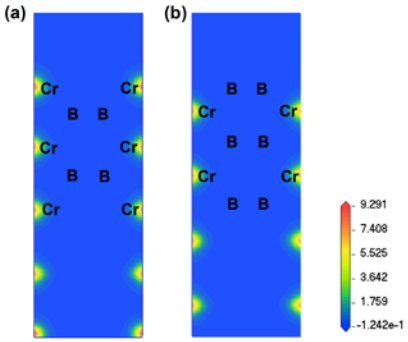

Figure 4. Spin density maps for (a) Cr-terminated and (b) B-terminated CrB_2 (0001) ultrathin films with nine atomic layers.

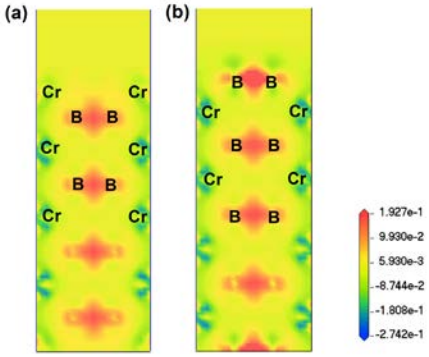

Figure 5. Difference charge density maps for (a) Cr-terminated and (b) B-terminated CrB_2 (0001) ultrathin films with nine atomic layers.

Summary

We report the first-principles investigation of CrB_2 (0001) freestanding ultrathin films based on density functional theory. The atomic, electronic and magnetic structures of Cr- and B-terminated thin films are studied in this paper. For both terminations, the interlayer spacings are contracted in most of the interlayer region. The outermost interlayer contraction of Cr-terminated films is larger than that of B-terminated ones because of the charge redistribution and binding nature. The charge transfer and spin moment from Mulliken population have also been analyzed. The results are well consist with the elucidation from the electron charge density maps. We find the presence of "pseudo-gap" existing in B-terminated systems and the splitting of peaks in the minority *s* and *p* spin states of Cr-terminated systems from DOS analysis. In addition, magnetic calculations demonstrate that the magnetism of CrB_2 ultrathin films is mainly contributed by Cr atoms and its thickness dependence is weak. It means changing of slab thickness does not significantly influence the magnetic properties of the CrB_2 ultrathin films; even films with slab thickness of 3 have big enough magnetic moments. This would make the controlled modification of the magnetism of CrB_2 thin films possible for real applications. Further studies of the influence of the substrate and the interactions between other materials would be necessary to clarify this point.

This work is supported by Education and teaching reformation program of liaoning province Project No:UPRP20140664.

Reference

[1] Novoselov KS, Geim AK, Morozov SV, Jiang D, Zhang Y, Dubonos SV, *et al*., Science 306 (2004) 666.

[2] Geim AK, Novoselov KS, Nat. Mater. 6 (2007) 183.
[3] Mas-Balleste R, Gomez-Navarro C, Gomez-Herrero J, Zamora F, Nanoscale 3 (2011) 20.
[4] Xu M, Liang T, Shi M, Chen H, Chem. Rev. 113 (2013) 3766.
[5] Butler SZ, Hollen SM, Cao L, Cui Y, Gupta JA, Gutierrez HR, *et al*., ACS Nano 7 (2013) 2898.
[6] Novoselov KS, Jiang D, Schedin F, Booth TJ, Khotkevich VV, Morozov SV, *et al*., Proc. Natl. Acad. Sci. USA 102 (2005) 10451.
[7] Ueno A, Fujita T, Matsue M, Yanagisawa H, Oshima C, Patthey F, *et al*., Surf. Sci. 600 (2006) 3518.
[8] Naguib M, Kurtoglu M, Presser V, Lu J, Niu J, Heon M, *et al*., Adv. Mater. 23 (2011) 4248.
[9] Naguib M, Mashtalir O, Carle J, Presser V, Lu J, Hultman L, *et al*., ACS Nano 6 (2012) 1322.
[10] Amo-Ochoa P, Welte L, Gonzalez-Prieto R, Sanz Miguel PJ, Go mez-Garcia CJ, Mateo-Marti E, *et al*., Chem. Commun. 46 (2010) 3262.
[11] Abel M, Clair S, Ourdjini O, Mossoyan M, Porte L, J. Am. Chem. Soc. 133 (2011) 1203.
[12] Coleman JN, Lotya M, O'Neill A, Bergin SD, *et al*., Science 331 (2011) 568.
[13] Zeng Z, Yin Z, Huang X, Li H, He Q, Lu G, *et al*., Angew. Chem. Int. Ed. 50 (2011) 11093.
[14] Patrick Vogt, Paola De Padova, Claudio Quaresima, Jose Avila, *et al*., Phys. Rev. Lett. 108 (2012) 155501.
[15] Antoine Fleurence, Rainer Friedlein, Taisuke Ozaki, Hiroyuki Kawai, *et al*., Phys. Rev. Lett. 108 (2012) 245501.
[16] Meng L, Wang Y, Zhang L, *et al*., Nano Lett. 13 (2013) 685.
[17] G. Brumfiel, Nature (London) 495 (2013) 152.
[18] Li L, Wang Y, Xie S, *et al*., Nano Lett. 13 (2013) 4671.
[19] O. Vaughan, Nat. Nanotechnol. 8 (2013) 699.
[20] Pinshane Y. Huang, Simon Kurasch, Anchal Srivastava, Viera Skakalova, *et al*., Nano Lett. 12 (2012) 1081.
[21] Zhao J, Deng Q, Alicja Bachmatiuk, Gorantla Sandeep, Alexey Popov, Jürgen Eckert, Science 343 (2014) 1228.
[22] C. Zhi, Y. Bando, C. Tang, H. Kuwahara, D. Golberg, Adv. Mater. 21 (2009) 2889.
[23] J.C. Meyer, A. Chuvilin, G. Algara-Siller, J. Biskupek, U. Kaiser, Nano Lett. 9 (2009) 2683.
[24] Wu X, Dai J, Zhao Y, *et al*., ACS Nano 6 (2012) 7443.
[25] Liu Y, Dr. Evgeni S. Penev, Prof. Boris I. Yakobson, Angew. Chem. Int. Ed. 52 (2013) 3156.
[26] P. Vajeeston, P. Ravindran, C. Ravi, R. Asokamani, Phys. Rev. B 63 (2001) 045115.
[27] K. Lie, R. Brydson, H. Davock, Phys. Rev. B 59 (1999) 5361.
[28] K. Lie, R. Høier, R. Brydson, Phys. Rev. B 61 (2000) 1786.
[29] H. Kawanowa, R. Souda, S. Otani, Y. Gotoh, Phys. Rev. Lett. 81 (1998) 2264.
[30] H. Kawanowa, R. Souda, K. Yamamoto, S. Otani, Y. Gotoh, Phys. Rev. B 60 (1999) 2855.
[31] J. Nagamatsu, N. Nakagawa, T. Muranaka, Y. Zenitani, J. Akimitsu, Nature (London) 410 (2001) 63.
[32] R.B. Kaner, J.J. Gilman, S.H. Tolbert, Mater. Sci. 308 (2005) 1268.
[33] W. Zhou, H. Wu, T. Yildirim, Phys. Rev. B 76 (2007) 184113.
[34] H.Y. Chung, M.B. Weinberger, J.B. Levine, A. Kavner, J.M. Yang, S.H. Tolbert, R.B. Kaner, Science 316 (2007) 436.
[35] R.W. Cumberland, M.B. Weinberger, J.J. Gilman, S.M. Clark, S.H. Tolbert, R.B. Kaner, J. Am. Chem. Soc. 127 (2005) 7264.
[36] I.R. Shein, A.L. Ivanovskii, Phys. Rev. B 73 (2006) 144108.
[37] V. Milman, B. Winkler, M.I.J. Probert, J. Phys.: Condens. Matter 17 (2005) 2233.
[38] H. Ihara, M. Hirabayashi, H. Nakagawa, Phys. Rev. B 16 (1977) 726.
[39] X. S. Song, S. J. Dong, H. Zhao, Comp. Mater. Sci. 84 (2014) 306.
[40] S. J. Dong, X. S. Song, H. Zhao, Phys. Lett. A 378 (2014) 1208.
[41] M.D. Segall, P.L.D. Lindan, M.J. Probert, C.J. Pickard, P.J. Hasnip, S.J. Clark, M.C. Payne, J. Phys.: Condens. Matter 14 (2002) 2717.
[42] P. Hohenberg, W. Kohn, Phys. Rev., 136B, 864 (1964).

[43] W. Kohn and L. J. Sham, Phys. Rev., 140A, 1133 (1965).
[44] J.P. Perdew, K. Burke, M. Ernzerhof, Phys. Rev. Lett. 77 (1996) 3865.
[45] I. V. Solovyev, M. Imada, Phys. Rev. B 71 (2005) 045103.
[46] Lei Wang, Thomas Maxisch, Gerbrand Ceder, Phys. Rev. B 73 (2006) 195107.
[47] I. S. Elfimov, A. Rusydi, S. I. Csiszar, Z. Hu, H. H. Hsieh, H.-J. Lin, C. T. Chen, R. Liang, G. A. Sawatzky, Phys. Rev. Lett. 98 (2007) 137202.
[48] I. Slipukhina, Ph. Mavropoulos, S. Blügel, M. Ležaić, Phys. Rev. Lett. 107 (2011) 137203.
[49] T.H. Fischer, J. Almlof, J. Phys. Chem. 96 (1992) 9768.
[50] D. Vanderbilt, Phys. Rev. B 41 (1990) 7892.
[51] H.J. Monkhorst, J.D. Pack, Phys. Rev. B 13 (1976) 5188.
[52] Wang S, Rikvold P A, Phys. Rev. B 65 (2002) 155406.
[53] Wang S, Cao Y, Rikvold P A, Phys. Rev. B 70 (2004) 205410.
[54] Wang F H, Liu S Y, Shang J X, Zhou Y S, Li Z Y, Yang J L, Surf. Sci. 602 (2008) 2212.
[55] Qin N, Liu S Y, *et al*., J. Phys.: Condens. Matter 23 (2011) 225501.
[56] Zhao H, Qin N, Appl. Surf. Sci. 258 (2012) 3328.
[57] M.D. Segall, R. Shah, C.J. Pickard, M.C. Payne, Phys. Rev. B 54 (1996) 16317.